

A Tool for Testing Conservation Properties in the COSMO-Model

M. BALDAUF

Deutscher Wetterdienst, Kaiserleistr. 42, D-63067 Offenbach am Main, Germany

1 Introduction

The fundamental equations of fluid mechanics, here especially those used in Meteorology can be formulated as conservation equations (or at least as balance equations) for mass, momentum and energy, as an example. Therefore an as good as possible conservation of these variables (or others, like enstrophy) should be obtained in a numerical model. Unfortunately this cannot be achieved in general but is guaranteed at most for a few variables in models which are formulated and also discretized in flux form. In all other cases it would be desirable to determine the strength of conservation violation.

To this purpose, a tool was developed to determine budgets of arbitrary scalar variables for the COSMO-Model (formerly known as LM). The budgets are calculated for an arbitrarily given cuboid volume inside of the model domain (see Figure 1).

This development was formulated as Task 3 in the COSMO-Priority Project 'Runge-Kutta'.

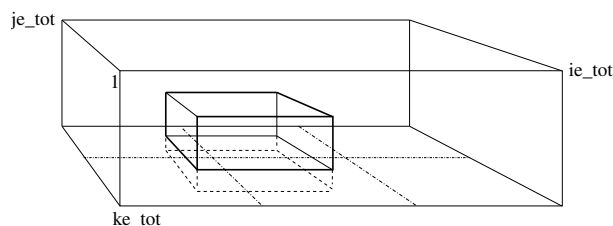


Figure 1: Integration area 'cuboid' lying in the model domain (in the transformed coordinate system). Here, a 3×2 domain decomposition is shown.

A general balance equation for a scalar ϕ (a generalized density) with an appropriate flux \mathbf{f}_ϕ sounds in integral form (i.e. over a steady volume V)

$$\begin{aligned}
 \frac{d}{dt}\Phi + F_\phi &= Q_\phi \\
 \text{total amount: } \Phi &:= \int_V \phi \, dv \\
 \text{total flux: } F_\phi &:= \int \int_{\partial V} \mathbf{f}_\phi \cdot d\mathbf{A} \\
 \text{all sinks/sources: } Q_\phi &:= \int_V q_\phi \, dv
 \end{aligned} \tag{1}$$

In the case of ϕ being an integral conservative variable the right side of the first equation vanishes and the residuum

$$Res := \frac{d\Phi}{dt} + F_\phi \tag{2}$$

describes the violation of conservation.

Consequently, for the determination of these budgets, one has to be able to calculate volume integrals and surface integrals over fluxes in the model. In Section 2 the numerical implementation of such a tool is described. In Section 3 the correct implementation is tested with

a strongly simplified test case. A first application is the determination of moisture balances in the Weisman-Klemp (1982)-Test in Section 4. Some remarks to implementation details and for the practical application is described in Section 5.

2 Numerical implementation

Calculation of the volume integral:

All the values of a variable in each grid element are weighted with the Jacobi-determinant D of the coordinate transformation and summed up

$$\Phi = \sum_{all\ GP \in V} \phi_{ijk} \cdot D_{ijk} \Delta V_{ijk} \quad (3)$$

where V denotes the volume of the cuboid, ΔV_{ijk} the volume of a grid cell in the transformed coordinate system, and D the Jacobi determinant

$$D := \left| \det \left(\frac{\partial x^i}{\partial \tilde{x}^j} \right) \right| = \frac{\partial x}{\partial \lambda} \cdot \frac{\partial y}{\partial \phi} \cdot \frac{\partial z}{\partial \zeta} \quad (4)$$

in the COSMO-model especially

$$\frac{\partial x}{\partial \lambda} = \frac{2\pi R_{Erd} \cos \phi}{360^\circ}, \quad \frac{\partial y}{\partial \phi} = \frac{2\pi R_{Erd}}{360^\circ}, \quad \frac{\partial z}{\partial \zeta} = -\sqrt{G} \quad (5)$$

\sqrt{G} is the metric weight of the terrain following coordinate transformation (Doms and Schättler, 2002).

Calculation of the surface integrals.

The surface integrals are directly calculated by

$$F_\phi = \sum_{all\ GP \in \partial V} \mathbf{f}_{ijk} \cdot \Delta \mathbf{A}_{ijk}. \quad (6)$$

where the summation is performed over all grid points at the surface of the cuboid volume V . It is assumed, that the flux components are defined at the same positions than the velocity components in the staggered grid: f_x at the u -position, f_y at the v -position and f_z at the w -position.

At the lateral boundaries it is sufficient to multiply the area of the surface element with the appropriate perpendicular flux component. Whereas at the top and bottom boundaries one has to obey that surface elements are skewly lying in general, due to the fact that the cuboid volume is terrain following. To consider this we are looking to such a surface element at the top, whose projection onto the x-y-plane is lying in the range $[0.. \Delta x, 0.. \Delta y]$, and which has a slope given by $\frac{\partial z}{\partial x}$ und $\frac{\partial z}{\partial y}$. This geometrically cuts out a rhomb, whose area can be calculated with Heron's formula to

$$dA = \sqrt{1 + \left(\frac{\partial z}{\partial x} \right)^2 + \left(\frac{\partial z}{\partial y} \right)^2} dx dy. \quad (7)$$

The square root term is exactly the length of the vector $(-\frac{\partial z}{\partial x}, -\frac{\partial z}{\partial y}, 1)$ and therefore the vector of the surface element at the top boundary reads

$$d\mathbf{A} = \begin{pmatrix} -\frac{\partial z}{\partial x} \\ -\frac{\partial z}{\partial y} \\ 1 \end{pmatrix}. \quad (8)$$

At the bottom boundary it is appropriately $-d\mathbf{A}$.

3 Shift-Tests

To test the abilities of the integration tool, a simple 'shift-test' is performed: an initial distribution is given and is transported with a constant velocity through the model domain. By doing this, one obviously assumes a perfect advection algorithm reconstructing the correct solution. In the continuous case one knows of course the correct distribution of the scalar and the appropriate flux. But on a discrete grid there occur some inaccuracies in the balancing of this process which will be called in the following the 'flux calculation artefact' and the 'volume calculation artefact'.

The volume integral and the flux integral over the surface do not cancel each other in general (see Figure 2). This cancellation only takes place for a transport with a Courant number $C = v\Delta t/\Delta x = 1$ and the usage of an upwind-scheme of 1st order for the fluxes using the field values from the time step before (see Table). For a Courant number of e.g. $C = 1/2$ this balance is not longer complete, which will be called here the 'flux calculation artefact'. But even in this case, the upwind-calculation of the fluxes seems to work best (see Table) and this will be used in the following exclusively.

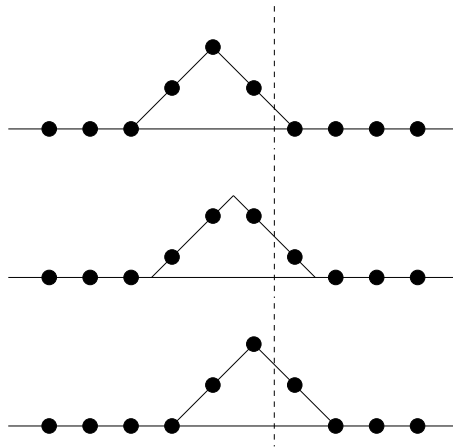


Figure 2: 'Shift-test'; explanation of the 'flux calculation artefact' at a Courant number $C = 1/2$.

| n | M^n | dM/dt | F_{up}^{n-1} | F_{up}^n | F_{cd}^{n-1} | F_{cd}^n |
|-----|-------|---------|----------------|------------|----------------|------------|
| 1 | 4 | 0 | 0 | 0 | 0 | 0 |
| 2 | 4 | 0 | 0 | 1 | 0 | 0.5 |
| 3 | 3 | -1 | 1 | 2 | 0.5 | 1.5 |
| 4 | 1 | -2 | 2 | 1 | 1.5 | 1.5 |
| 5 | 0 | -1 | 1 | 0 | 1.5 | 0.5 |
| 6 | 0 | 0 | 0 | 0 | 0.5 | 0 |
| 7 | 0 | 0 | 0 | 0 | 0 | 0 |
| ... | | | | | | |

Table 1: Shift-Test (see also the upper and lower pictures in Figure 2): transport with $v = 1 \cdot \Delta x/\Delta t$, M^n is the total mass in the integration volume at the time step t^n , F_{up} is the integral over the flux divergence with an upwind-scheme 1st order, F_{cd} with centered differences 2nd order, where the fields are used either at time step t^n or at time step t^{n-1} .

| n | M^n | dM/dt | F_{up}^{n-1} | F_{up}^n | F_{cd}^{n-1} | F_{cd}^n |
|-----|-------|---------|----------------|------------|----------------|------------|
| 1 | 4 | 0 | 0 | 0 | 0 | 0 |
| 2 | 4 | 0 | 0 | 0.25 | 0 | 0.125 |
| 3 | 4 | 0 | 0.25 | 0.5 | 0.125 | 0.25 |
| 4 | 3.5 | -0.5 | 0.5 | 0.75 | 0.25 | 0.5 |
| 5 | 3 | -0.5 | 0.75 | 1 | 0.5 | 0.75 |
| 6 | 2 | -1 | 1 | 0.75 | 0.75 | 0.75 |
| ... | | | | | | |

Table 2: Shift-Test (see Figure 2): transport with $v = 1/2 \cdot \Delta x / \Delta t$, for denotations see Table .

An other numerical problem, called the 'volume calculation artefact' arises even when the boundaries are not crossed. Assume that a distribution of the form $y = (1 - x)^2$, if $y > 0$, 0 otherwise is given on a grid with $\Delta x = 1$. If this distribution is shifted with a velocity $v = 1/2 \Delta x / \Delta t$ through the grid, then the 'total mass' fluctuates between the two values $M = 1$ and $M = 1.5$ (see Figure 3). This means even if no boundary of the integration volume is crossed by the distribution there can occur a mass change in every time step. In this case obviously a temporal mean cures this problem to a certain extent (in this example, the correct integral value is $M = 4/3 = 1.333\dots$) Therefore it seems to be reasonable to carry out a temporal integration over the residuum (2)

$$\Delta\Phi = \int_{t_a}^{t_e} Res dt. \quad (9)$$

In the following, the quotient $\Delta\Phi/\Phi$ is called the *relative error*.

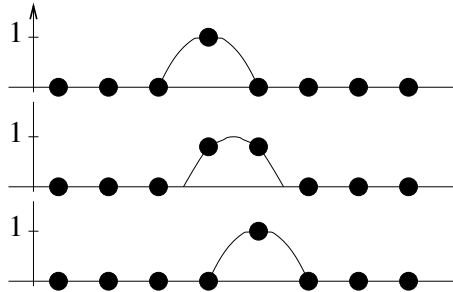


Figure 3: 'Shift-Test': 'volume calculation artefact'. The calculated masses alternate between $M = 1$ (top, bottom) and $M = 1.5$ (middle) from time step to time step.

'Shift-Test' with the integration tool: After these preliminary considerations the integration tool of the COSMO model itself will now be inspected by the 'Shift-Test'. An elliptical '3D-cone distribution' serves as initialisation:

$$f_{cone}(x, y, z) := \begin{cases} 1 - r & : r < 1 \\ 0 & : r \geq 1 \end{cases}, \quad r := \sqrt{\left(\frac{x}{a}\right)^2 + \left(\frac{y}{b}\right)^2 + \left(\frac{z}{c}\right)^2}, \quad (10)$$

whose volume integral is

$$M := \frac{\pi}{3} a \cdot b \cdot c. \quad (11)$$

Shift-Test 1: The grid length is *exactly* $\Delta x = \Delta y = \Delta z = 500$ m with the transport velocity $v = 5$ m/s (in each coordinate direction $+x, -x, +y, \dots$), and a time step $\Delta t = 100$ s.; this means in every time step the distribution is transported by exact one grid length. For the present no orography is used ($h = 0$).

| | M | dM/dt | D | Res | delta M |
|------|----------------|----------------|---------------|----------------|----------------|
| ... | | | | | |
| n= 3 | 0.6703411E+11 | 0.0000000E+00 | 0.0000000E+00 | 0.0000000E+00 | 0.0000000E+00 |
| n= 4 | 0.6703411E+11, | 0.7629395E-07 | 0.0000000E+00 | 0.7629395E-07 | 0.7629395E-05 |
| ... | | | | | |
| n=23 | 0.6703411E+11 | 0.0000000E+00 | 0.0000000E+00 | 0.0000000E+00 | -0.1005852E-20 |
| n=24 | 0.6703411E+11 | 0.0000000E+00 | 0.0000000E+00 | 0.0000000E+00 | -0.1005852E-20 |
| n=25 | 0.6667258E+11 | -0.3615338E+07 | 0.3615338E+07 | 0.1001172E-06 | 0.1001172E-04 |
| n=26 | 0.6536316E+11 | -0.1309420E+08 | 0.1309420E+08 | -0.2123415E-06 | -0.1122244E-04 |
| n=27 | 0.6271460E+11 | -0.2648554E+08 | 0.2648554E+08 | 0.9313226E-07 | -0.1909211E-05 |
| n=28 | 0.5852479E+11 | -0.4189810E+08 | 0.4189810E+08 | 0.1266599E-06 | 0.1075678E-04 |
| n=29 | 0.5279093E+11 | -0.5733864E+08 | 0.5733864E+08 | -0.1341105E-06 | -0.2654269E-05 |
| n=30 | 0.4571720E+11 | -0.7073733E+08 | 0.7073733E+08 | 0.1937151E-06 | 0.1671724E-04 |
| n=31 | 0.3770282E+11 | -0.8014380E+08 | 0.8014380E+08 | -0.1043081E-06 | 0.6286427E-05 |
| n=32 | 0.2933130E+11 | -0.8371522E+08 | 0.8371522E+08 | 0.1490116E-06 | 0.2118759E-04 |
| n=33 | 0.2131692E+11 | -0.8014380E+08 | 0.8014380E+08 | 0.1490116E-07 | 0.2267770E-04 |
| n=34 | 0.1424318E+11 | -0.7073733E+08 | 0.7073733E+08 | 0.5960464E-07 | 0.2863817E-04 |
| n=35 | 0.8509318E+10 | -0.5733864E+08 | 0.5733864E+08 | 0.1490116E-07 | 0.3012829E-04 |
| n=36 | 0.4319508E+10 | -0.4189810E+08 | 0.4189810E+08 | 0.1490116E-07 | 0.3161840E-04 |
| ... | | | | | |

Table 3: Shift-test 1; total mass M , its change in one timestep $\Delta M/\Delta t$, the surface integral of the fluxes D , residuum Res and its temporal sum ΔM .

Table 3 shows the result for a transport in $-x$ -direction. As long as the cone lies in the interior of the cuboid, the volume integrals M are identical up to machine accuracy (up to time step $n = 24$). They are even exactly identical ($dM/dt = 0$), as long as the cone lies in the interior of one processor domain (up to $n = 3$). When processor domain boundaries are crossed by the distribution there occurs an error by the summation over all processors in the order of the machine accuracy. When crossing the boundary of the cuboid the surface integrals are almost exactly balanced with the mass change and the relative error $\Delta M/M$ is only about 10^{-14} . For a transport in $+x, -y, +y, -z, +z$ -direction the results are almost identical. A domain decomposition with 3×2 processors was used, therefore the parallelisation of the integration tool seems to work properly.

Shift-test 2: As Shift-test 1, but now the (very small!) curvature of the earth surface is considered ($\text{crlat}(:, :) \neq 1$). Even in this small integration area there occurs a relative error of about 10^{-7} .

Shift-test 3: As Shift-test 1, but with the half of the velocity ($v = 2.5$ m/s in all 6 coordinate directions), i.e. in every time step the cone distribution will be transported about exactly $1/2$ grid length. The errors are rather big in the meantime (Figure 4) and even at the end of the transport, when the distribution lies outside of the integration cuboid, the relative error is about $|\Delta M/M_0| \approx |-0.514 \cdot 10^7 / 0.670 \cdot 10^{11}| \approx 10^{-4}$. This is clearly due to the 'flux calculation artefact' where the mass changes and the sum of the fluxes over the boundaries do not cancel each other. For a transport in $+x, -y, +y, -z, +z$ -direction the results are looking almost exactly the same. The reason is that we do not see any longer the roundoff errors but the truncation error which is nearly the same in all directions.

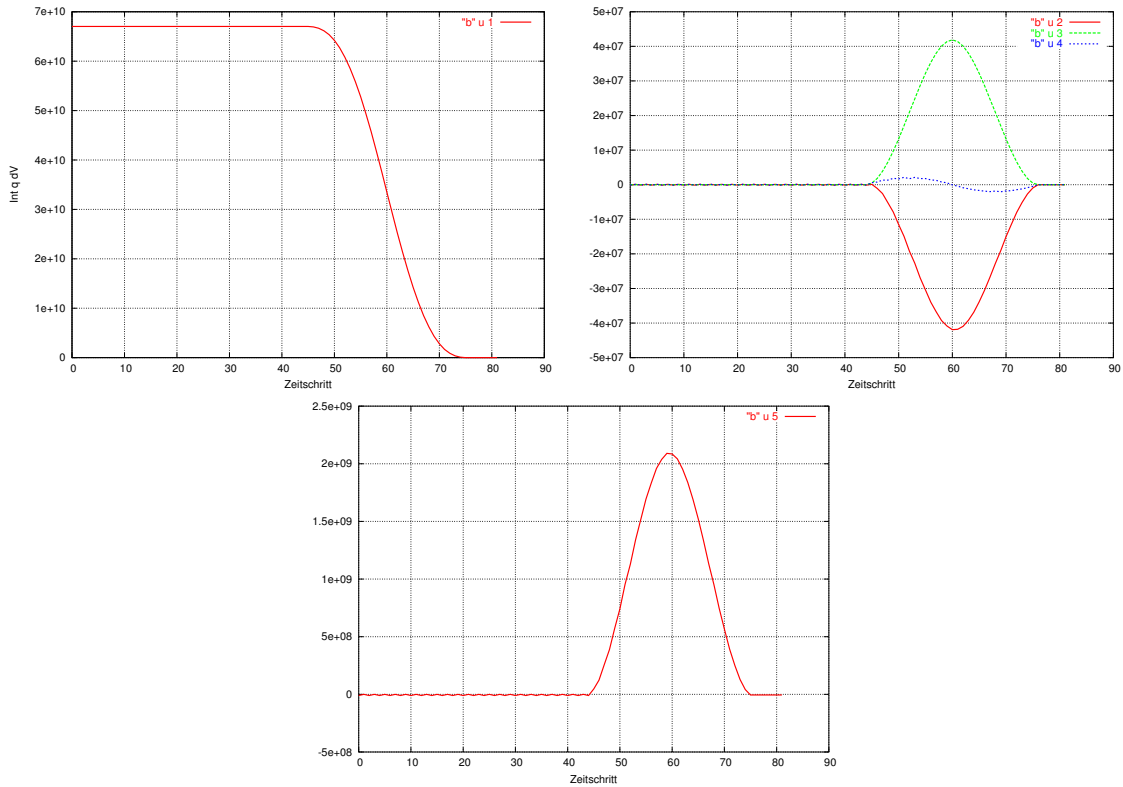


Figure 4: 'Shift-Test 3', Mass of moisture variables Φ (above, left), above, right: the balance terms $\Delta\Phi/\Delta t$ (red), F_ϕ (green), and the residuum (blue); below, left: the temporal integral of the residuum ΔM .

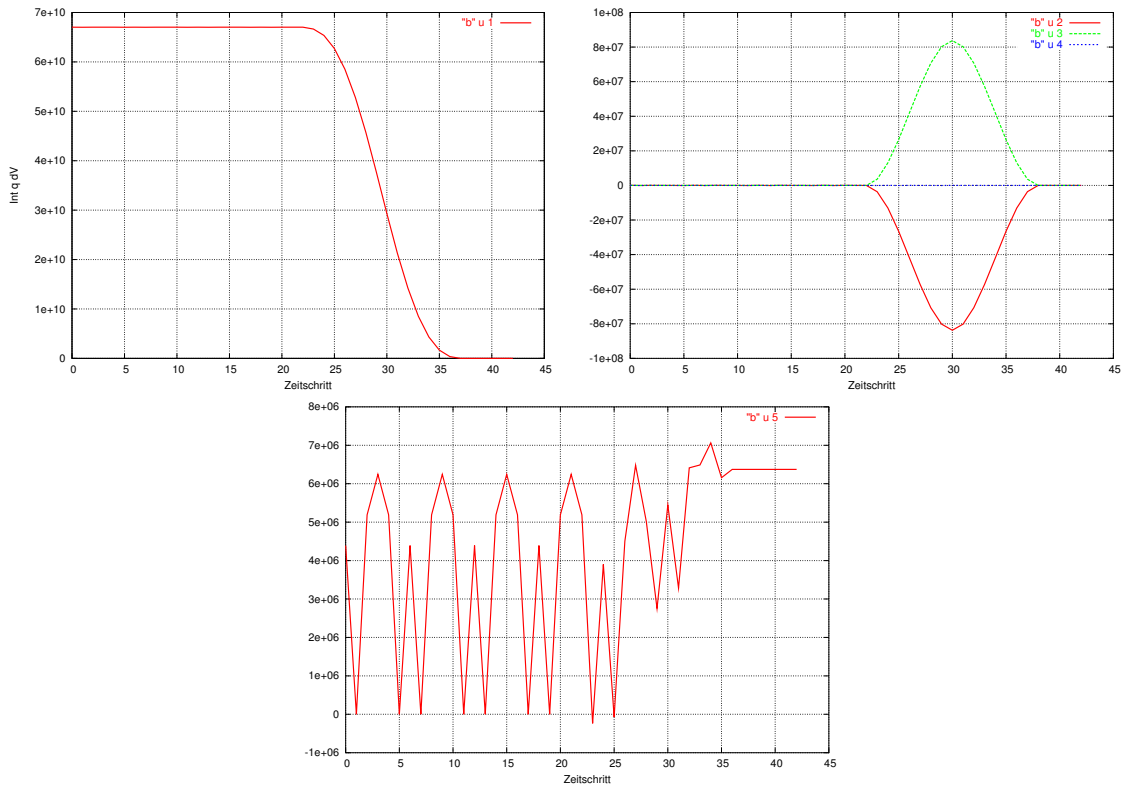


Figure 5: 'Shift-Test 4', denotations as in Figure 4.

Shift-test 4: As Shift-test 1, but with orography (sinus hill lines with $h = 500\text{m}$ and $L = 12dx = 6\text{km}$). Figure 5 shows, that the relative error is about 10^{-4} . It is in the same order of magnitude for a transport in z-direction; this indicates that the somewhat more complicated surface integral over the top and bottom boundary of the cuboid seems to work. For a transport in the other space directions there is a little bit more direction dependence of the results which comes from a stronger asymmetry (compared to shift-test 1) induced by the orography.

4 The Weisman-Klemp test case

A first application of the integration tool was carried out with the idealised Weisman-Klemp-test case (Weisman and Klemp, 1982). An ellipsoidal warm bubble serves as an initial disturbance with a maximum increase of temperature of $\max \Delta T = 2\text{ K}$, whose center lies in a height of 1400 m and which has the radii 10000 m , 10000 m , 1400 m (therefore it just touches the ground).

The horizontal grid length is $\Delta x = \Delta y = 2\text{ km}$, and the time step $\Delta t = 10\text{ sec}$. The atmosphere is in steady state at the beginning. The physics parameterisations are completely switched off, only the saturation adjustment (condensation and evaporation) is active. Therefore only water vapour q_v and cloud water q_c can occur, i.e. the density of total water is

$$\rho_x = \rho(q_v + q_c).$$

Further on there occur only advective fluxes $\mathbf{v}\rho_x$, but no turbulent or sedimentation fluxes.

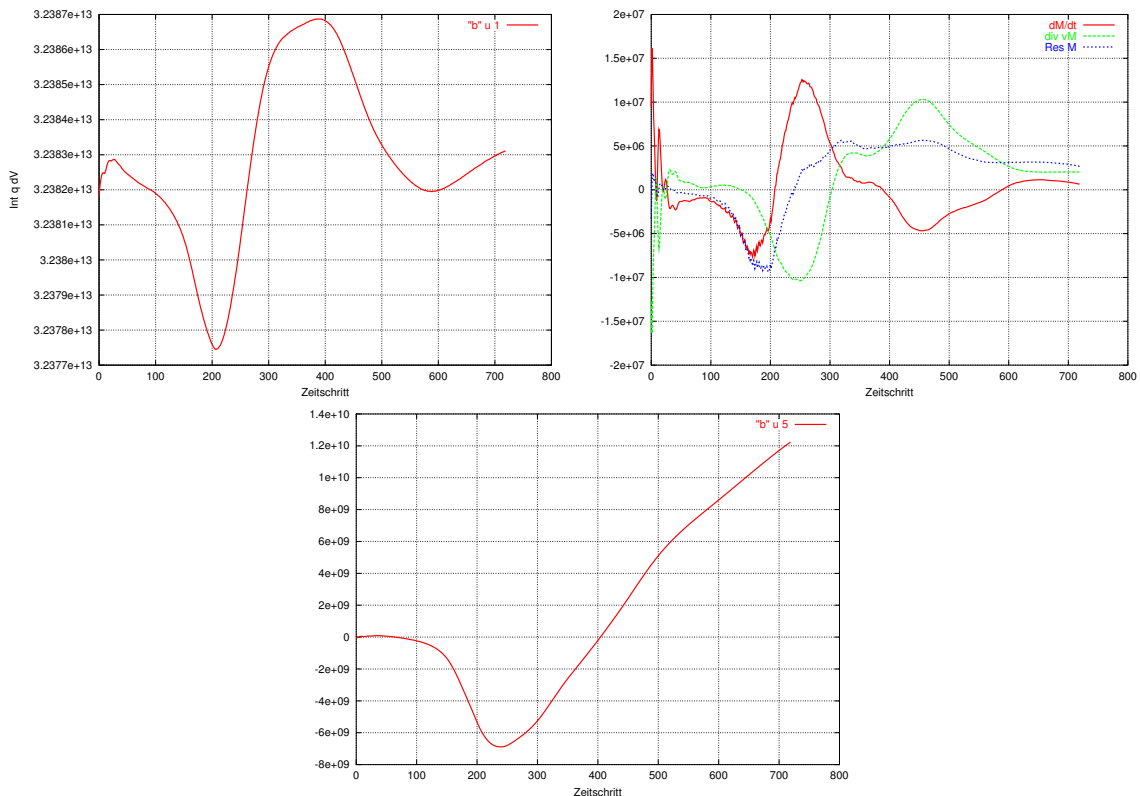


Figure 6: Exp. WK1: Weisman-Klemp-test case, density ρ , total mass M (left), temporal integral of the residuum ΔM (right).

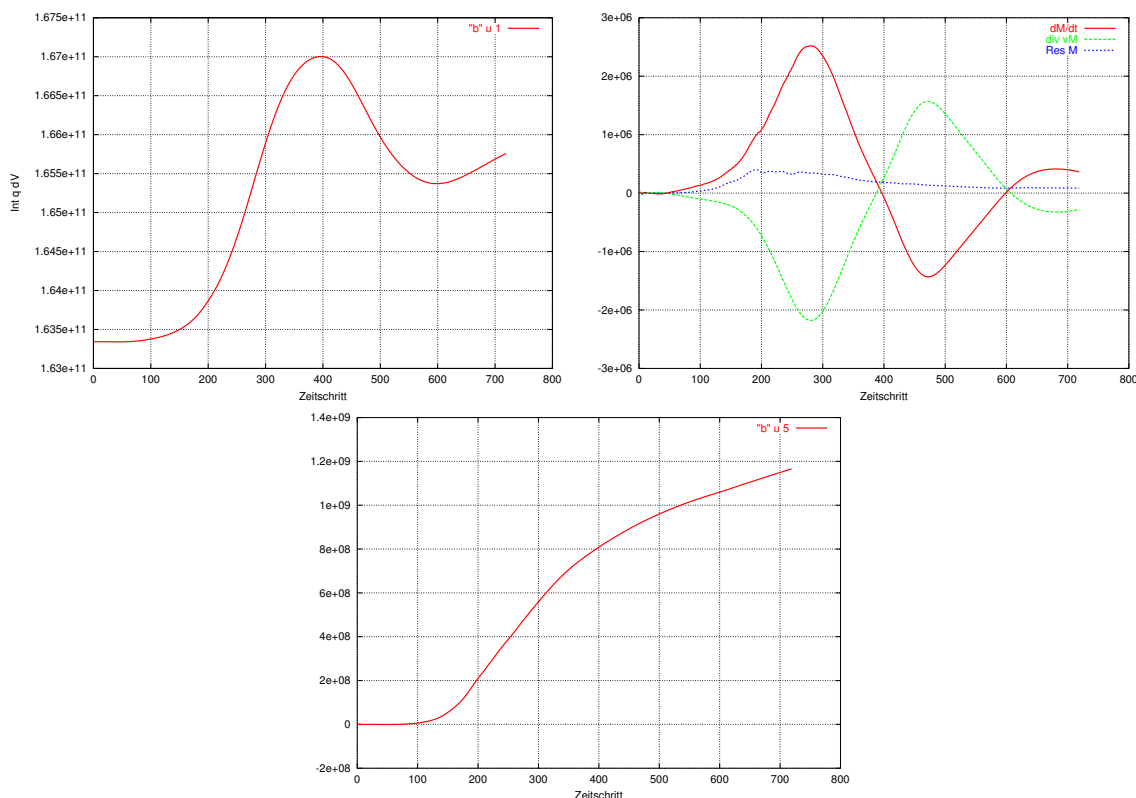


Figure 7: Exp. WK1: Weisman-Klemp-test case, density of moisture $\rho_x = \rho(q_v + q_c)$, total mass of moisture Φ (above, left), above, right: balance terms $\Delta\Phi/\Delta t$ (red), F_ϕ (green) and the residuum (blue), and the temporal integral of the residuum ΔM (below).

The moisture transport is carried out with a Semi-Lagrange-advection scheme with a tricubic interpolation (Baldauf, 2004), in which the mass conservation is guaranteed globally by a multiplicative filling (Rood, 1987). There were also carried out experiments with the Bott-advection scheme (Förstner et al., 2006) for which the following results are mainly the same.

The integration area was chosen in a manner, that no relaxation boundary zone is crossed. Of course, relaxation zones destroy any conservation property (the upper relaxation zone starts in $z = 13700$ m; the upper boundary of the cuboid lies in $k_{min}=10$, i.e. in $z = 12900$ m. The lateral Davies-relaxation zone has a width of 20 km, i.e. 10 grid points).

Figure 6 shows the total mass of the first experiment (Exp. WK1). There exist a certain mass conservation violation indicated by the the residuum (blue line in the upper right picture) and by its temporal integration (lower picture) leading to a relative error of $1.2 \cdot 10^{10} \text{ kg} / 3.24 \cdot 10^{13} \text{ kg} \approx 0.04\%$.

In Figure 7 the balance of the moisture mass is shown. During the rising of the bubble (approximately the first 400 timesteps) moist air is sucked especially from the lower portions of the atmosphere. When the buoyancy is reduced, the bubble expands sideways and blows out the moist air (timesteps 400-600). During this process the positive tendency of the mass change is not very well balanced by the negative tendency of the flux divergence (and vice versa); the residuum is rather big (upper left picture in Figure 7). And therefore the relative error is about $1.2 \cdot 10^9 \text{ kg} / 1.65 \cdot 10^{11} \text{ kg} \approx 0.7\%$.

Therefore the question arises if this is a real error in the model or an artefact by the inte-

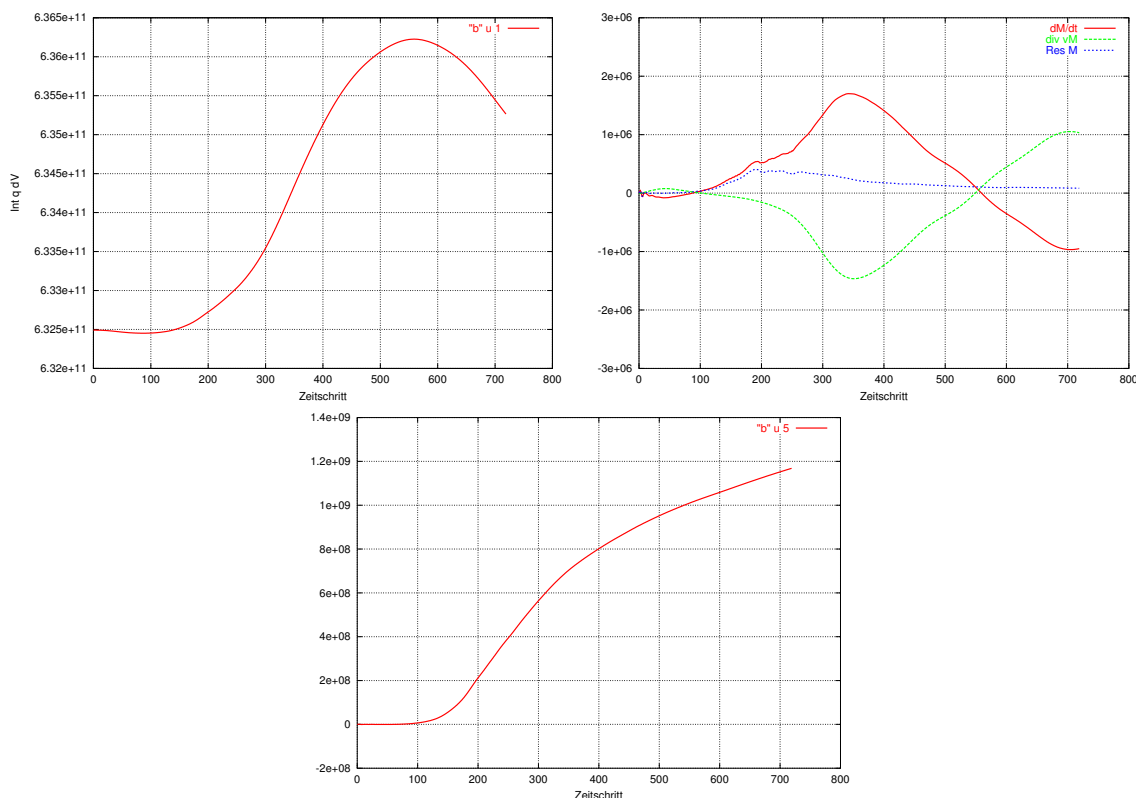


Figure 8: Exp. WK8: denotations are the same as in Figure 7.

gration tool. Because the Bott-advection scheme delivers very similar results, the problem seems not to be due to the advection scheme. The error in the total mass calculation of the above mentioned 0.04% seems to be too small to explain this moisture mass change.

To reduce artefacts by the calculation of the flux integrals the integration area was increased by a factor of 2 in x- and y-direction (experiment WK8). The upper left picture in Figure 8 shows the nearly 4 times more moisture mass compared to the case WK1. Due to the bigger integration area the signal of the rising bubble arrives later at the integration boundaries and therefore the temporal slope of the moisture mass and the balance terms seems to be stretched compared to case WK1, although the physical process of the rising bubble is exactly the same than in WK1. The only signal which is nearly the same and therefore independent of the integration box, is the residuum. This indicates, that the violation of the conservation is not induced by the inflow through the boundaries, but there seems to be a violation of conservation by the description of the physical process by the model.

To inspect this assumption, the saturation adjustment was switched off in experiment WK9. Because the buoyancy is drastically reduced due to the lack of latent heat release, a much warmer bubble was chosen; otherwise it would not rise very high. Here the temperature perturbation was increased from 2K to 10K.

In Figure 9 the residuum is (apart from the first few timesteps), clearly closer to zero than in experiment WK8. This also shows the sufficient conservation property of the Semi-Lagrange-advection in this case. The only cause then for violation of conservation seems to be the saturation adjustment. Indeed, the saturation adjustment in the COSMO-model conserves the specific mass (and specific energy) but not mass (and energy) themselves.

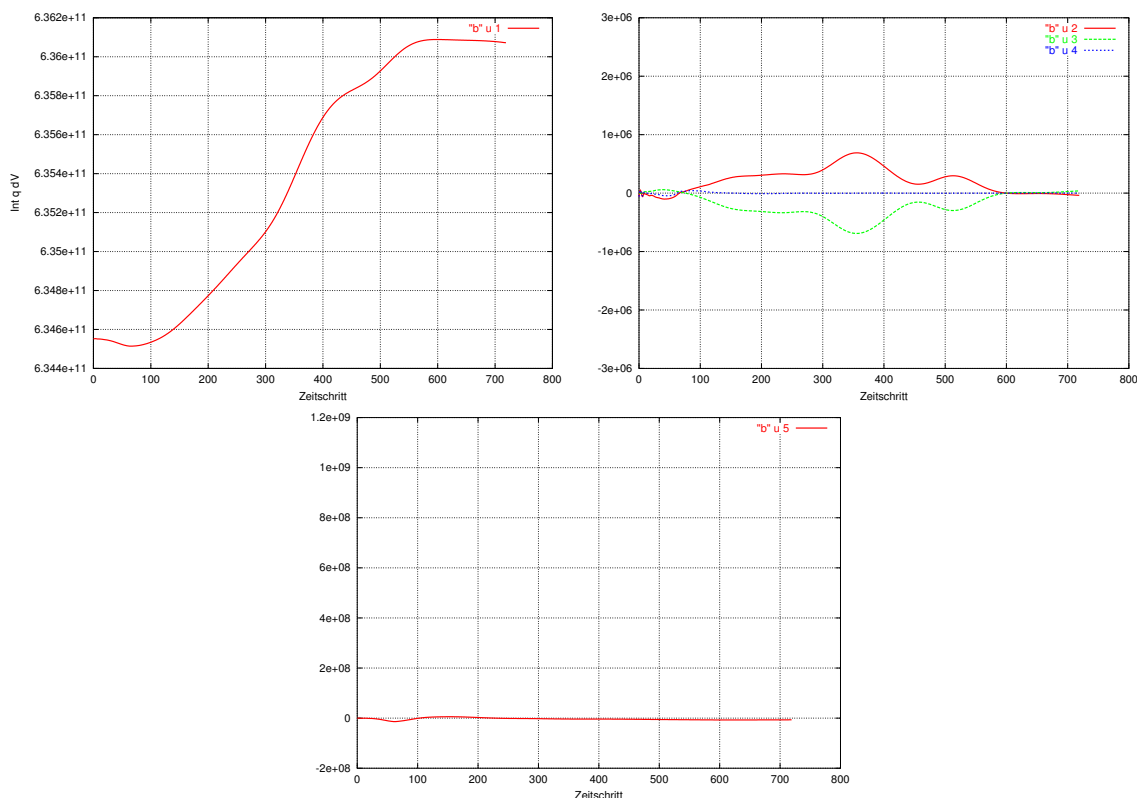


Figure 9: Exp. WK9: Weisman-Klemp-test case with a '10K bubble', without condensation, denotations are the same as in Figure 7.

5 Implementation

The integration tool is activated by the NAMELIST-switch `l_integrals`. The coordinates of the cuboid corners `imin_integ`, `imax_integ`, `jmin_integ`, `jmax_integ`, `kmin_integ`, `kmax_integ` are read from the NAMELIST-parameter group `DIACTL`. If they are not set, then the whole COSMO-model area is used as the integration area by default (be aware of relaxation boundary zones then) The module `src_integrals` in file `src_integrals.f90` contains the following subroutines: in `init_integral_3d` the data structure 'integ_cuboid' (of type `cuboid_multiproz_type`) is initialised. Especially the domain decomposition of the cuboid and the location of its surfaces appropriate to the domain composition of the model domain is carried out there. `integral_3d_total` calculates the volume integral over the cuboid and `surface_integral_total` calculates the 6 surface integrals over the N-, S-, O- and W-boundary and over the top and bottom boundary. Subroutine `calc_sqrtg_r_s` delivers the metric coefficient $1/\sqrt{G}$ at the location of the scalars (this is needed only in the 3-timelevel version, the 2-timelevel version calculates it automatically).

The basic subroutine for organizing the computations is `organize_integrals` (`yaction`). The parameter `yaction` can take one of the three values 'init', 'compute', or 'final'.

A first example for the calculation of total mass conservation is done by the subroutine `check_rho_conservation`. It calls as an example for calculating purely advective fluxes $\mathbf{F} = \rho \cdot \mathbf{v}$ (which only arise in the continuity equation) the subroutine `adv_fluxes_upwind`.

6 Conclusions

A tool to calculate balances in the COSMO-model was developed. Although such a tool itself has some inherent sometimes misleading properties as was discussed in Section 3, it can be used successful at least in idealised simulations and can give valuable hints for the violation of conservation properties. Here the boundaries often can be set far away from the interesting physical process and therefore the 'flux calculation artefact' can be reduced. Up to now no experiences with the application in real case simulations were made. For example, the Weisman-Klemp test showed an rather constant increase in total mass. It would be interesting to inspect this behaviour further on in real case studies.

References

- Baldauf, M., 2004: The Lokal-Modell (LM) of DWD / COSMO. *Proceedings of ECMWF: Recent developments in numerical methods for atmospheric and ocean modelling*, 6.-10. September 2004, <http://www.ecmwf.int/publications/library/do/references/list/161>, 41–52.
- Doms, G., U. Schättler, 2002: *A Description of the Nonhydrostatic Regional Model LM, Part I: Dynamics and Numerics*, Offenbach, Germany; Deutscher Wetterdienst.
- Förstner, J., M. Baldauf, A. Seifert, 2006: Courant Number Independent Advection of the Moisture Quantities for the LMK. *COSMO-Newsletter*, No. 6, 51–64.
- Rood, R., 1987: Numerical advection algorithms and their role in atmospheric transport and chemistry models. *Rev. Geophys.*, **25** (1), 71–100.
- Weisman, M., J. Klemp, 1982: The dependence of numerically simulated convective storms on vertical wind shear and buoyancy. *Mon. Wea. Rev.*, **110**, 504–520.